# Biometric Recognition via Probabilistic Spatial Projection of Eye Movement Trajectories in Dynamic Visual Environments

Ioannis Rigas, *Member*, *IEEE*, Oleg V. Komogortsev, *Member*, *IEEE*

***Abstract*—This paper proposes a method for the extraction of biometric features from the spatial patterns formed by eye movements during an inspection of dynamic visual stimulus. In the suggested framework each eye movement signal is transformed into a time-constrained decomposition by using a probabilistic representation of spatial and temporal features related to eye fixations and called Fixation Density Map (FDM). The results for a large collection of eye movements recorded from 200 individuals indicate the best equal error rate (EER) of 10.8% and Rank-1 identification rate (Rank-1 IR) as high as 51%, which is a significant improvement over existing eye movement-driven biometric methods. In addition, our experiments reveal that a person recognition approach based on the FDM performs well even in cases when eye movement data are captured at lower than optimum sampling frequencies. This property is very important for the future ocular biometric systems where existing iris recognition devices could be employed to combine eye movement traits with iris information for increased security and accuracy. Considering that commercial iris recognition devices are able to implement eye image sampling usually at a relatively low rate, the ability to perform eye movement-driven biometrics at such rates is of great significance.**

***Index Terms*—Behavioral biometrics, eye movement cues, Fixation Density Maps, security enhancement.**

## I. Introduction

BIOMETRICS RESEARCH has rapidly progressed during the last decades, endeavoring to find the most appropriate characteristics that express human individuality as well as the mathematical models for their representation and comparison. Biometric technologies that rely on distinctive features such as fingerprints [1], iris [2], and face [3] have reached a maturity level, delivering high identification rates and receiving widespread adoption. Nevertheless, the stable structure of these features, which is the reason of their high accuracy, appears also as their Achilles' heel, since they are easily susceptible to forgery and various types of spoofing attacks [4], [5]. This is one of the reasons that fed the necessity for exploring other methods of personal identification, ranging from regular approaches as hand geometry [6] and palm-print [7] biometrics to more sophisticated techniques, such as vein pattern authentication [8]. Furthermore, biometric research moved towards characteristics that encapsulate not only physical but also behavioral cues of individuals. Hand-writing dynamics [9] and voice recognition [10] can be considered among the primary fields of study, whereas other sources of behavioral features include keystroke dynamics [11] and gait [12].

Applications of biometric technology were for a long time a privilege of military or government security agencies. However, the last few years a turning point is clearly observed with the increasing adoption of biometric-related technologies in common-use appliances. Some characteristic examples include face recognition utilities recently added in personal laptops, fingerprint authentication modules introduced in the latest smartphones, and the voice recognition systems incorporated in modern cars. The widespread endorsement of biometric technologies in everyday-life applications urges for an investigation of novel biometric traits that could be easily integrated in human-centered environments. In this context, eye movements appear as a potentially precious source of characteristics considering the current trend for user-friendly touchless appliances, capable of interacting with face region [13]. Eye movements encapsulate both physical and behavioral information. Their dynamic nature renders them a suitable security enhancement option (e.g. for liveness detection [14]) in multi-modal schemes based on more classic features, such as the iris [15]. Additionally, since recording of eye movements is accomplished from the face region, extracted characteristics may be combined with other established biometric traits captured from the same area, such as periocular [16], nose [17], and lip biometrical cues [18].

### A. Characteristics of Eye Movements

Movement of the eye globe is accomplished by a system of six extra-ocular muscles, acting as agonist/antagonist pairs: the superior and inferior rectus are primarily responsible for the execution of the vertical component of movements, the lateral and medial rectus generate the horizontal component of eye movements and the superior and inferior oblique are employed primarily for the execution of the torsional movement components. Eye movements are coordinated by the neuronal control signal from the brain [19] which guides them to hold the eyes at positions of interest (fixations) and to rapidly move them from one fixation point to another by executing stereotypical, ballistic movements called saccades.

Manuscript received January 18, 2014; revised April 01, 2014; accepted June 02, 2014. This work is supported in part by NSF CAREER Grant #CNS-1250718 and NIST Grants #60NANB10D213 and #60NANB12D234. Special gratitude is expressed to Dr. E. Abdulin, T. Miller, and Ch. Heinich for proctoring eye movement recordings.

Dr. I. Rigas is with the Department of Computer Science, Texas State University, San Marcos, TX 78666 USA (e-mail: rigas@txstate.edu)

Dr. O. V. Komogortsev is with the Department of Computer Science, Texas State University, San Marcos, TX 78666 USA (phone: 512-245-0349; fax: 512-245-8750; e-mail: ok11@txstate.edu)

Active visual observation is a procedure modulated both by bottom-up attention mechanisms, activated from features such as color, orientation, texture, and by top-down factors resulting from a cognitive task, e.g., object-oriented visual search [20]. Due to this duality (low-level attraction/perceptual modulation) eye movement features incorporate both physiological and behavioral traits. The physical traits of eye movements correspond to the geometrical properties of the ocular system (shape of the eyes, pupil size), the parameters of the mechanical plant defined by the extraocular muscles (passive elasticity, active state tension, length tension relationship, series elasticity, force velocity relationship), and neuronal control signal frequency characteristics [21]. The behavioral aspects, on the other hand, arise from the individual's brain activity that defines "where and how" the eyes are going to move during cognitive tasks. The formation of idiosyncratic repetitive patterns during visual inspection was initially explored during the experiments of Noton and Stark [22], [23] in 1971. Their research led to the Scanpath Theory, stating that during the inspection of a specific visual stimulus eye movements form patterns (scanpaths), which can be partially replicated during the subsequent observations of the same stimulus. These patterns are potentially influenced by the stimulus, the mental task, and the individual attention strategy of each person. The validity of Scanpath Theory is confirmed by several scientific studies [24], [25], [26]. These research efforts were conducted for different visual tasks, and the resulting findings indicate the presence of a varying degree of similarity for the scanpaths formed by the same person. However, there are also cases that failed to capture any degree of similarity [27]. The results of the research presented in [28] were mixed, since in some cases idiosyncratic patterns were observed, whereas in others the stimulus influence strongly modulated eye movement signals.

### B. Related Work

The first research effort exploring eye movement features in the field of biometrics was presented in [29]. In this work, Cepstrum transform was used for the investigation of unique characteristics that could be enfolded into the spectral components of eye movements. The experimental results for a database of 9 subjects reported 1% false acceptance rate (FAR) and 23% false rejection rate (FRR).

The field of voice recognition served as a source of inspiration for the method developed in [30]. The specific research was motivated by the existing analogies in the behavioral nature of eye movement and speech signals, and the implemented model was optimized with the use of training signals of variable lengths. The best-achieved performance for a database of 17 subjects provided an EER of 29.4%.

A mathematical framework for the description and analysis of eye movements based on extra-ocular muscles and neural control signal parameters, the Oculomotor Plant Characteristic (OPC), was presented in [31]. The evaluation experiments, implemented with the participation of 59 subjects, revealed a minimum half total error rate (HTER) of 19%.

In [32], the efficiency of graph matching techniques was tested on a set of eye movement recordings captured under the influence of a cognitive visual stimulus (human faces). The achieved identification rate (Rank-1 IR) for a database of 15 subjects was 70%, whereas the reported EER was 30%.

Recently, the corrective mechanisms of the oculomotor system were explored as a possible source of idiosyncratic traits. The extracted characteristics constituting the Complex Oculomotor Behavior (COB) [33], were found to enclose useful personal information, as demonstrated by the performances of 25% EER and 47% Rank-1 IR for a set of 32 subjects.

In [34], an objective evaluation for the Complex Eye Movement (CEM) features previously introduced in [35] was presented and evaluated using databases of different size, recorded with devices of various specifications. The best results for a database of 32 subjects and a high-resolution device (1000 Hz) were 28% EER and 38% Rank-1 IR, whereas the respective rates for a database of 22 subjects and a device operating at 300 Hz were 31% EER and 53% Rank-1 IR. For low-resolution equipment (75 Hz) and a database of 173 persons EER was 34% and Rank-1 IR 7%. An expansion of the CEM framework was proposed in [36], achieving rates of 16.5% EER and 83.7% Rank-1 IR for the high-quality database of 32 subjects and 25.6% EER and 16.3% Rank-1 IR for the low-quality database of 173 subjects.

### C. Motivation & Hypothesis

The basis of the developed scheme lies on an idea that during observation of a complex dynamic visual stimulus (e.g. video sequence), spatial and temporal fixation characteristics would be indicative of the brain activity related to the generation and guidance of visual attention, thus providing an opportunity to identify a person based on such activity. This idea is based on the concept that the brain is responsible for encoding information for "where and how" an eye is going to move given specific stimulus, and thus spatial locations of the fixations, their duration, and order can be employed to decode part of this information. Decoded information forms a biometric template that represents part of the brain activity in a mathematical form. To build this representation we implement a projection of the raw time-sampled eye movement signal into the spatial domain. Then, we construct multi-map biometric templates using generated Fixation Density Maps (FDMs), representing person's attention activity for sequential time intervals. This representation possesses the following important properties: 1) spatial distributions of fixation samples are represented in a robust way, 2) possible overlap effects for attention-drawing regions are diminished, and 3) implicit incorporation of time evolution characteristics for the recorded trajectory is possible.

FDM biometrics were previously introduced in [37]. Our current work greatly extends on the research related to FDM biometrics since:

a) A generalized framework is presented for the FDM-based comparison of eye movement patterns in the presence of dynamic cognitive visual stimulus. Our research includes the exploration of different comparison measures for FDMs and the usage of fusion schemes for information combination.

b) The experiments were conducted with the use of a larger

database consisting of 200 subjects, making it the largest considered eye movement database to date.

c) Our work explores the possibility of employing enrollments from different visual content in order to enhance performance, and dynamically update the biometrical templates.

d) We investigate the relative tolerance of the proposed method to the degradation in temporal resolution and compare the obtained performance with methods outlined in the related work section.

## II. Representation of Eye Movements with Fixation Density Maps

Spatial projection of the eye movement trajectories is implemented by using the Fixation Density Map (FDM) as a basic structural element. Let us assume that an eye tracking device captures eye movement samples with a sampling frequency $f_s$. Then, for a specific recording time interval $T_{int}$ a FDM can be constructed with the following procedure: for an individual fixation point, let $\Delta\theta_i$ (Fig. 1) denote the angle formed by visual axis for the fixation point $i$ with regard to axis direction when it crosses the screen center. If we denote with $\Delta\theta x_i$, $\Delta\theta y_i$ the angles corresponding to the horizontal and vertical projection of the visual axis, then using the experimental setting geometry—the viewing distance $d_s$ is assumed known and fixed—we may calculate the coordinates for the distances $\Delta x_i$, $\Delta y_i$ from the center as:

$$\Delta x_i = tan(\Delta\theta x_i \cdot \pi/180^0) \cdot d_s \quad (1)$$

$$\Delta y_i = tan(\Delta\theta y_i \cdot \pi/180^0) \cdot d_s \quad (2)$$

By employing the known values for the stimulus screen dimensions ($h_s$, $w_s$) and resolution ($h_p$, $w_p$), we may in turn convert the distances from the center to the respective pixel coordinates $(x_i, y_i)$ by using the translation equations:

$$x_i = (w_s/2) + (w_s/w_p) \cdot \Delta x_i \quad (3)$$

$$y_i = (h_s/2) + (h_s/h_p) \cdot \Delta y_i \quad (4)$$

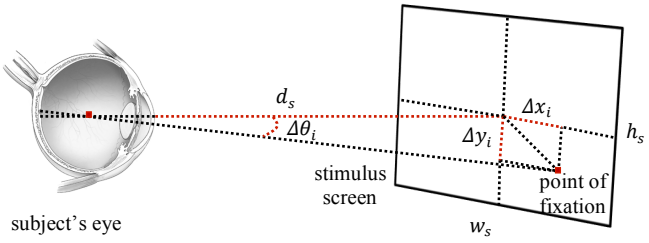


Fig. 1. Optical geometry of the experimental configuration used for gaze recording.

During the next step, we construct a discrete map (DCM) from the fixation samples by representing each sample with a unitary spike in the corresponding pixel location:

$$DCM(x,y) = \sum_{i=1}^{K} \delta(x - x_i)(y - y_i), \; K = T_{int} \cdot f_s \quad (5)$$

In order to transform the discrete map into a probabilistic representation, we apply a Gaussian kernel of standard deviation σ and construct the final Fixation Density Map:

$$FDM(x,y) = DCM(x,y) * G_\sigma(x,y) \quad (6)$$

A value of σ = 0.02 (normalized in map's width) is globally used during our implementation. This value was selected so that it corresponds—under our experimental settings—to the average receptive area of the eye's fovea, which is roughly 1° of visual angle [38].

A FDM can be regarded as a 2-D imprint of the temporal evolution of attention in the space of the specific visual stimulus. In case of a dynamic stimulus, e.g., a video sequence, there are two basic factors which need to be considered: i) the spatial layout of the visual content changes over time and ii) visual inspection may last for an extended period of time (depending on the video duration). Consequently, if a single FDM is constructed for the representation of eye movements during a long recording, there might be overlapping fixations that complicate analysis. Moreover, a single representation cannot capture temporal eye movement characteristics which represent important information related to the individual guidance of visual attention. To overcome this, we propose a procedure that involves a decomposition of each eye movement signal into parts corresponding to sequential time intervals. For every recording, with a total duration of $T_R$, the raw eye movement signal is initially partitioned into $n$ equal-duration ($T_{int}$) non-overlapping sequential segments. In our implementation we use an interval of $T_{int}$ = 5 seconds. This empirically selected duration ensured that a robust sequence of fixations and saccades is captured without significant overlapping effects for the selected stimulus. A separate FDM is constructed for every segment and the final biometric template is formatted by concentrating all of the constructed FDMs into a multi-map representation. During the template matching phase the respective map components are pairwise compared, therefore, correctly aligning temporal and spatial information encoded in the eye movements by the brain and oculomotor plant. Fig. 2 presents a brief visual summary of the described procedure.

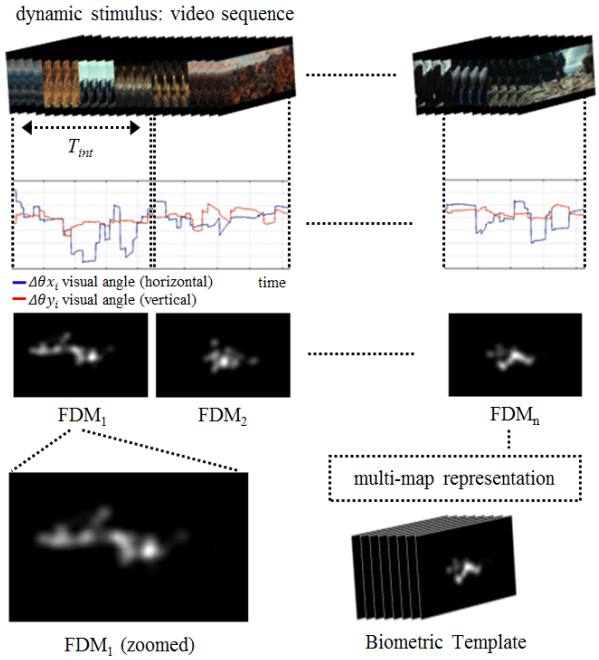

## III. Comparison of Fixation Density Maps

### A. Similarity Measures for Fixation Density Maps

In the field of visual attention modeling, several different schemes have been proposed for the comparison of map representations of visual prominent features, generally known as low-level saliency maps [38], [39]. In the case of FDMs, instead of using the visual content information the map is constructed by directly employing the eye movement samples coming from a person. Due to the morphological similarity between saliency maps and FDMs, we explore the efficacy of four different map comparison measures originating from the field of visual saliency for the task of biometrical recognition via FDMs.

*Similarity metric (SIM)*

This measure has been suggested in an attention modeling scheme [40] as a simple approach for measuring the commonly activated areas between two saliency maps. In order to use it in our framework we assume that the FDMs under comparison correspond to two distributions $P(x,y)$ and $Q(x,y)$. Then, the Similarity metric can be calculated by finding the minimum value between the two distributions under consideration at every spatial location and sum all respective values.

$$SIM(P,Q) = \sum_{x=1}^{N}\sum_{y=1}^{M} min\big(P(x,y), Q(x,y)\big) \quad (7)$$

The two distributions are assumed to be normalized to sum to unity, $\sum_{x=1}^{N}\sum_{y=1}^{M} P(x,y) = 1$, $\sum_{x=1}^{N}\sum_{y=1}^{M} Q(x,y) = 1$, where $N$, $M$ = width and height of the maps.

*Pearson's Correlation Coefficient r (PCC)*

The Pearson's Correlation Coefficient $r$ can be defined as the ratio that expresses the degree of covariance between two variables relative to the mean of their individual variances. The correlation coefficient ranges from -1 to 1, with 0 denoting no correlation between two variables, 1 denoting strong correlation in the same direction, and -1 indicating strong correlation in opposite directions. Assuming that the FDMs $P(x,y)$ and $Q(x,y)$ are the variables under consideration, we may use the *PCC* as a gauge of the correlation between them. *PCC* can be calculated using the following formula:

$$PCC(P,Q) = \frac{\sum_x\sum_y P\cdot Q - \frac{\sum_x\sum_y P\cdot\sum_x\sum_y Q}{N.M}}{\sqrt{\left[\sum_x\sum_y P^2 - \frac{\left(\sum_x\sum_y P\right)^2}{N\cdot M}\right]\left[\sum_x\sum_y Q^2 - \frac{\left(\sum_x\sum_y Q\right)^2}{N\cdot M}\right]}} \quad (8)$$

*Kullback-Leibler Divergence (KLD)*

The Kullback-Leibler Divergence [41] is a measure to express the overall dissimilarity between two probability density functions by calculating the relative entropy of one of them with respect to the other. If we denote $p$, $q$, the probability density functions that correspond to FDMs $P(x,y)$ and $Q(x,y)$, then the Kullback-Leibler Divergence can be calculated as:

$$KLD(P,Q) = \sum_{x=1}^{N}\sum_{y=1}^{M} q(x,y)\cdot log\left(\frac{q(x,y)}{p(x,y)}\right) \quad (9)$$

with $\sum_x\sum_y p(x,y) = 1$, $\sum_x\sum_y q(x,y) = 1$, and additionally $p(x,y) > 0$ for any $x$, $y$ such that $q(x,y) > 0$.

Due to the fact that the relative entropy of $P(x,y)$ relative to $Q(x,y)$ has a different value than $Q(x,y)$ relative to $P(x,y)$, the Kullback-Leibler Divergence produces non-symmetric similarity matrices, and additionally the calculated values lack a well-defined upper boundary. We will describe below a procedure implemented to overcome these deficiencies and use the *KLD* for the comparison of FDMs.

*Earth Mover's Distance (EMD)*

The measure of Earth Mover's Distance can be used for the computation of the distance between two probability distributions over a region by calculating the minimal cost for the transformation of one distribution to the other. During our experiments we employed the implementation of *EMD* developed by Judd *et al.* [40]. By representing FDMs as distributions $P(x,y)$, $Q(x,y)$, the Earth Mover's Distance can be calculated by solving the well-known transportation problem [42]. If we denote $f_{i,j}$ the transported amount from the $i^{th}$ supply to the $j^{th}$ demand, and $d_{i,j}$ the ground distance between the $i^{th}$ and the $j^{th}$ bin in distribution, the Earth Mover's Distance is computed with the use of the following equation:

$$EMD(P,Q) = \min_{f_{ij}}\left(\sum_{i,j} f_{i,j}\cdot d_{ij}\right) + \left|\sum_i P_i - \sum_j Q_j\right|\cdot \max_{i,j} d_{i,j} \quad (10)$$

under the restrictions: $f_{i,j} \geq 0$, $\sum_j f_{ij} \leq P_i$, $\sum_i f_{ij} \leq Q_j$, and $\sum_{i,j} f_{i,j} = min\left(\sum_i P_i - \sum_j Q_j\right)$.

As stated above, the Kullback-Leibler Divergence produces non-symmetric similarity matrices and lacks the upper bound. The latter property is also a feature of Earth Mover's Distance. Motivated by the work in the field of classification in dissimilarity space [43], [44], we decided to develop an Euclidean space embedding procedure for the employed dissimilarity measures, so that we can use them for the comparison of biometric templates. Let us denote $D$ the full $S\times S$ matrix that contains the dissimilarity values calculated for $S$ different samples. If $D_L$ is the lower triangle of the full matrix, then we can use these values in order to construct a symmetric matrix ($D_S$):

$$D_s = D_L + (D_L)^T - diag(D) \quad (11)$$

Considering each row of the new matrix as a feature of the dissimilarity space we can calculate their Euclidean distances, resulting thus in a normalized Euclidean distance matrix ($D_{Final}$) which is symmetrical and has a well-defined upper bound:

$$D_{Final}(i,j) = \frac{D_{Eucl}(i,j)}{\max_{i,j} D_{Eucl}}, i,j = 1,\dots,S \quad (12)$$

with $D_{Eucl} = EuclideanDistance(D_S, (D_S)^T)$.

This matrix can be used during the classification procedure in our biometric scenarios.

### B. Fusion of Information from Fixation Density Maps

In the above description we presented similarity measures for the pairwise comparison of the maps that correspond to

respective time intervals of a video sequence. Since biometric templates consist of multiple maps, we need to effectively combine the information coming from the map components that correspond to different time intervals. In the case of FDMs, each component correlates with the spatio-temporal layout of the visual input, making thus a direct combination of information on the feature level infeasible. For this reason, we perform information fusion in the match score level, by combining the generated matching scores for every time interval into a single score which expresses the overall similarity between two templates. In our experiments, we implemented and assessed the following fusion schemes:

*(SM) Simple Mean.* This is the simplest method that is used for fusing the match score information. A simple linear combination with equal weights is computed over the similarity scores that correspond to different FDMs in order to generate a single matching score in the interval [0,1].

*(WM) Weighted Mean.* The weighted mean algorithm uses a slightly more complicated approach by utilizing a number of training samples in order to perform an iterative error minimization procedure using the genuine and impostor samples. During this process a vector of different weights is generated and then used for the linear combination of the match scores coming from the corresponding FDMs.

*(LR) Likelihood Ratio.* This fusion algorithm initially builds a set of Gaussian mixture models by using information from a training set [45]. Subsequently, it generates a model by calculating likelihood ratio of the genuine samples over the imposter samples and uses this model for the combination of the individual match scores into a single value in the interval [0, ∞].

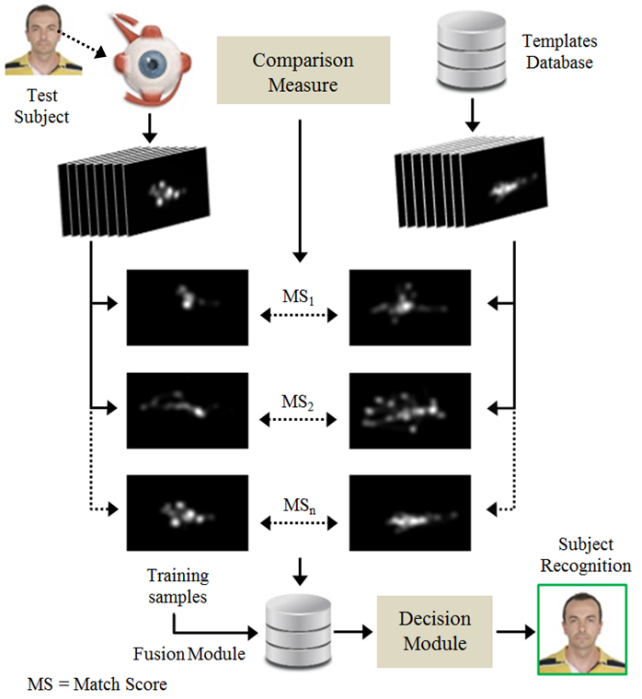


Fig. 3. Overview of the architecture of the developed biometric recognition scheme based on FDM templates.

Fig. 3 illustrates the various parts of the proposed approach for the implementation of a biometric recognition system based on FDM comparison.

## IV. Experimental Methodology

### A. Visual Stimulus

The eye movement recording experiment was conducted with the employment of a time-changing cognitive stimulus consisting of video sequences. Specifically, the official trailer of the Hollywood film "Hobbit 2: The Desolation of Smaug (2013)" was used. This video sequence was selected due to the variety of its content, consisting of rapidly changing action scenes, static parts with emotional content, and briefly presented text banners. The trailer was partitioned into two different segments of approximate duration of 1 minute each. During the experiments, every participant enrolled separately for each of these video segments, leading to the formation of the two independent datasets of eye movement recordings VD1 and VD2. Our decision for partitioning the video sequence instead of using it as a whole is supported by the following arguments:

a) An extensive visual stimulus presentation might lead to mental fatigue which in turn may influence negatively the behavioral characteristics of eye movements.

b) A recording with a large duration would lead to excessively large number of features (in our case many FDMs), thus increasing the computational burden.

c) Performance may be investigated for the combination of FDM templates generated from videos of different content.

It must be noted that the recordings for VD1 and VD2 were a part of a larger experiment where subjects performed various eye movement tasks with several periods of rest to reduce possible fatigue effects. The time gap between VD1 and VD2 recording was approximately 20 minutes. Several other tasks and brief rest periods between those tasks were performed by the subject between VD1 and VD2 related recordings. Total duration of all tasks and periods of rest did not exceed 1 hour.

### B. Participants

The experiments for the formation of the eye movement datasets employed in this work were conducted with the participation of 200 subjects (93 males, 107 females), ages 18-44 with an average age of 22 (SD = 4.08). Every subject performed two recordings for each video segment, yielding a collection of totally 800 unique eye movement samples. Texas State University's institutional review board approved the study, and every participant provided informed consent.

### C. Apparatus

Eye movement recordings were accomplished with the use of an EyeLink 1000 eye tracker [46] running at 1000 Hz, with vendor's reported spatial accuracy 0.5°. The specific device implements two pupil tracking algorithms, the Centroid and the Ellipse fitting. The preferred mode was the Centroid, a method which uses a center of mass algorithm for tracking the center of the thresholded pupil. In Fig. 4, example images are provided demonstrating pupil tracking, captured via the interface of the employed experimental device.

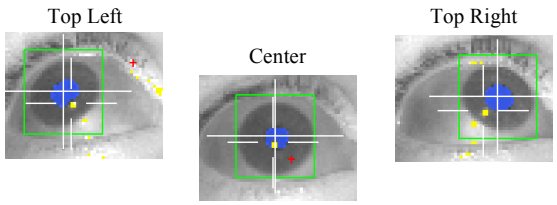


Fig. 4. Images of the tracked pupil for different eye gaze positions. The tracked corneal reflection can also be observed as a (yellow) dot.

The device was positioned at a distance of 550 millimeters from the computer screen, with dimensions of 474 x 297 millimeters and resolution of 1680 x 1050 pixels. The head of each subject was comfortably stabilized by using a chin rest with a forehead bar. During our experiments, the average measured calibration accuracy for the recorded datasets was 0.49° (SD = 0.17°), whereas the average recorded data validity was determined to 96.08% (SD = 5.20%).

## V. Results

All performance rates reported in this section are obtained by splitting the database samples into training and testing sets, with a 50%-50% partitioning according to a uniformly random distribution and average the results over 20 random partitions. In the presented figures, the data were fitted to a quadratic polynomial curve by using MATLAB function *fit*.

### A. Verification Scenario

A *genuine score* refers to a similarity value for two samples generated from the same identity. An *impostor score* refers to a similarity value for two samples generated from different identities. A general overview of the separation degree for these two populations (*genuine*/*impostor*) is possible by inspecting the distributions formed by the respective scores. Fig. 5 depicts the distributions formed by *genuine* and *impostor scores* generated during the comparison of FDM templates, for the case of dataset VD1.

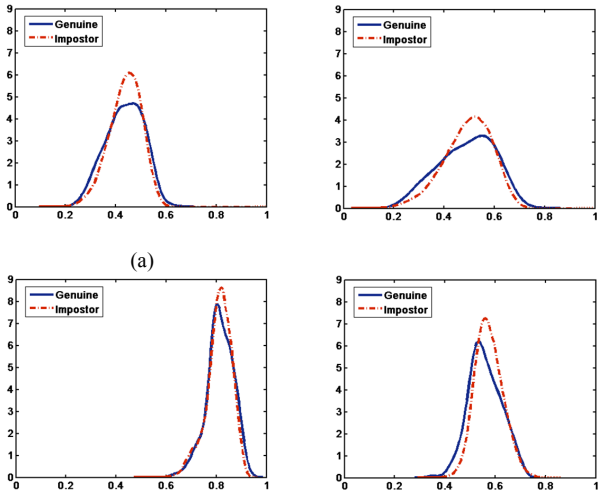


Fig. 5. Distributions of *genuine* and *impostor scores* for comparison measures: (a) *SIM*, (b) *PCC*, (c) *KLD*, and (d) *EMD*) (*SM* fusion scheme was used).

By defining an acceptance threshold ($\eta$) we can compute the False Positive Rate (FPR) as the percentage of the *genuine scores* that fall under the threshold $\eta$ and the False Acceptance Rate (FAR), as the percentage of the *impostor score*s that are over $\eta$. True Positive Rate (TPR) can be defined as the percentage of *genuine scores* that are over the threshold $\eta$, and it stands TPR = 1 - FPR. By changing the acceptance threshold and calculating the respective values for TPR and FAR, we can construct a Receiver Operating Characteristic (ROC) curve, which allows for a general inspection of the biometric system's trade-off between correct identification and impostor intrusion. One way for summarizing the information of a ROC curve is by calculating Equal Error Rate (EER). Equal Error Rate corresponds to the point of operation where the False Positive Rate equals the False Acceptance Rate. In Table I, we may observe the calculated Equal Error Rates for each of the comparison measures used for FDMs, for datasets VD1 and VD2. The table contains the individual rates for the maps that correspond to each time interval (M01-M11) and the final performances after match score fusion. The best performance in every case is highlighted. For dataset VD1, a one-way ANOVA reveals no significant main effect for EER across different time intervals, $F(10, 33) = 0.7$, $p = 0.7178$, but there is a significant main effect across comparison measures, $F(3, 40) = 29.96$, $p < 0.001$. These results are verified from the analysis for VD2, with the respective values across different time intervals being $F(10, 33) = 0.99$, $p = 0.4691$ and across comparison measures $F(3, 40) = 26.77$, $p < 0.001$.

TABLE I

EQUAL ERROR RATES

| | VD1 | | | | | VD2 | | | |
|---|---|---|---|---|---|---|---|---|---|
| **Feat.** | **Comparison Measure** | | | | **Feat.** | **Comparison Measure** | | | |
| | ***SIM*** | ***PCC*** | ***KLD*** | ***EMD*** | | ***SIM*** | ***PCC*** | ***KLD*** | ***EMD*** |
| *M01* | **30.9%** | 33.5% | **24.6%** | 30.8% | *M01* | **33.0%** | **34.4%** | **24.5%** | **25.6%** |
| *M01* | 38.5% | 38.2% | 26.2% | 35.0% | *M01* | 35.9% | 37.4% | 28.8% | 29.4% |
| *M03* | 37.0% | 40.6% | 27.0% | 34.6% | *M03* | 34.6% | 35.4% | 26.6% | 32.9% |
| *M04* | 35.6% | 38.3% | 26.5% | 34.7% | *M04* | 33.2% | 34.9% | 29.1% | 32.7% |
| *M05* | 34.4% | 37.0% | 29.5% | 30.4% | *M05* | 35.9% | 36.7% | 25.8% | 31.8% |
| *M06* | 41.4% | 42.4% | 28.6% | 31.2% | *M06* | 35.1% | 35.2% | 26.6% | 31.9% |
| *M07* | 38.5% | 39.4% | 30.0% | 31.6% | *M07* | 40.1% | 40.8% | 30.1% | 39.8% |
| *M08* | 35.9% | 34.4% | 31.8% | 31.0% | *M08* | 37.1% | 36.3% | 31.3% | 32.3% |
| *M09* | 31.8% | **32.3%** | 25.4% | **29.4%** | *M09* | 37.7% | 38.1% | 31.2% | 35.3% |
| *M10* | 34.1% | 36.4% | 27.6% | 30.8% | *M10* | 40.2% | 40.2% | 29.2% | 33.9% |
| *M11* | 36.1% | 37.3% | 27.8% | 29.6% | *M11* | 38.2% | 39.2% | 24.8% | 33.1% |
| **Fusion** | | | | | **Fusion** | | | | |
| *SM* | 26.7% | 28.1% | 20.2% | 16.5% | *SM* | 27.9% | 29.6% | 22.6% | 18.3% |
| *WM* | 27.7% | 29.5% | 23.0% | 23.8% | *WM* | 31.0% | 31.9% | 24.5% | 22.2% |
| *LR* | **25.8%** | **27.7%** | **19.9%** | **12.1%** | *LR* | **27.4%** | **29.1%** | **21.9%** | **13.6%** |

In Fig. 6, we present the constructed ROC curves for both datasets used during our experiments. Using these curves we may obtain a more general view of the characteristics of the used comparison measures. The curves were constructed by using the calculated rates for the best performing fusion scheme, which is the Likelihood Ratio (*LR)* in all cases.

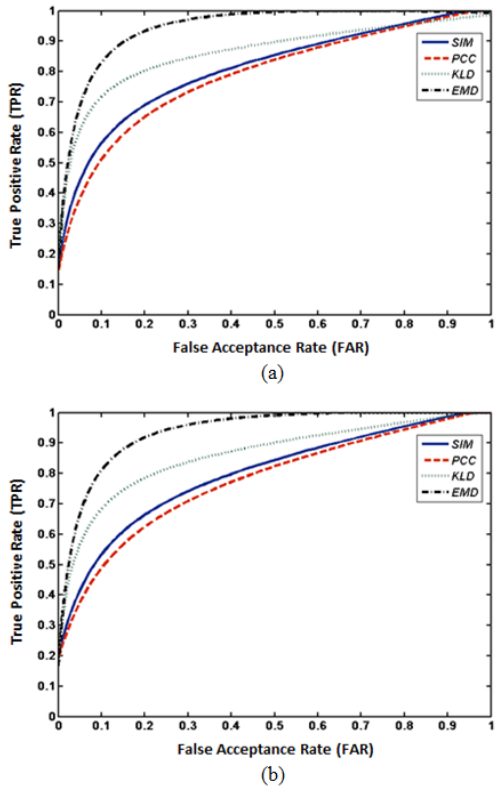


Fig. 6. Receiver Operating Characteristic (ROC) curves for datasets (a) VD1 and (b) VD2 (using *LR* fusion scheme).

### B. *Identification Scenario*

Rank-*k* Identification Rate (Rank-*k* IR) is a measure of accuracy, which shows the percentage of *genuine scores* that can be found within the *k* top matches of a biometric system. Table II shows the calculated values for Rank-1 IR for the individual maps that correspond to each time interval and the total performance after the combination of the individual match scores.

TABLE II

RANK-1 IDENTIFICATION RATES

| Feat. | VD1 Comparison Measure | | | | Feat. | VD2 Comparison Measure | | | |
|---|---|---|---|---|---|---|---|---|---|
| | ***SIM*** | ***PCC*** | ***KLD*** | ***EMD*** | | ***SIM*** | ***PCC*** | ***KLD*** | ***EMD*** |
| *M01* | 7.6% | 5.1% | **26.9%** | 13.0% | *M01* | 8.9% | 7.1% | 23.6% | 14.9% |
| *M01* | 5.2% | 3.6% | 16.4% | 11.1% | *M01* | 8.4% | 6.1% | 18.1% | **16.7%** |
| *M03* | 7.9% | 5.3% | 18.4% | 8.8% | *M03* | 8.6% | 8.0% | 23.3% | 11.4% |
| *M04* | 5.6% | 2.9% | 25.0% | 12.6% | *M04* | **10.3%** | **9.9%** | 23.7% | 14.0% |
| *M05* | 5.2% | 4.7% | 14.7% | 14.6% | *M05* | 8.5% | 5.7% | 25.9% | 14.7% |
| *M06* | 3.0% | 2.8% | 17.1% | 14.0% | *M06* | 7.4% | 6.5% | **26.0%** | 15.3% |
| *M07* | 6.7% | 5.3% | 19.7% | 15.1% | *M07* | 4.1% | 3.3% | 18.5% | 7.2% |
| *M08* | 7.8% | 8.2% | 19.9% | 13.6% | *M08* | 9.6% | 6.7% | 23.6% | 15.9% |
| *M09* | **11.1%** | **8.6%** | 25.2% | **17.5%** | *M09* | 5.6% | 4.4% | 22.9% | 12.7% |
| *M10* | 8.4% | 6.0% | 18.3% | 13.8% | *M10* | 5.1% | 4.3% | 18.7% | 10.0% |
| *M11* | 5.2% | 4.7% | 19.4% | 15.8% | *M11* | 5.9% | 4.3% | 15.6% | 10.4% |
| **Fusion** | | | | | **Fusion** | | | | |
| *SM* | 28.7% | 23.0% | **39.4%** | 25.0% | *SM* | 30.2% | **26.2%** | **38.0%** | 26.7% |
| *WM* | 20.5% | 14.6% | 28.4% | 16.8% | *WM* | 15.6% | 13.9% | 27.5% | 19.9% |
| *LR* | **29.9%** | **23.1%** | 36.2% | **32.5%** | *LR* | **31.8%** | **26.2%** | 31.8% | **32.8%** |

A one-way ANOVA for Rank-1 IR indicates no significant main effect across different time intervals both for dataset VD1, $F(10, 33) = 0.28$, $p = 0.9810$, and for dataset VD2, $F(10, 33) = 0.36$, $p = 0.9552$. As previously, there is a significant main effect across comparison measures, with the respective values for dataset VD1, $F(3, 40) = 70.89$, $p < 0.001$ and for dataset VD2, $F(3, 40) = 78.81$, $p < 0.001$.

The evolution of identification rates as a function of the employed rank *k* is computed and demonstrated using the Cumulative Match Characteristic (CMC) curves, shown in Fig. 7.

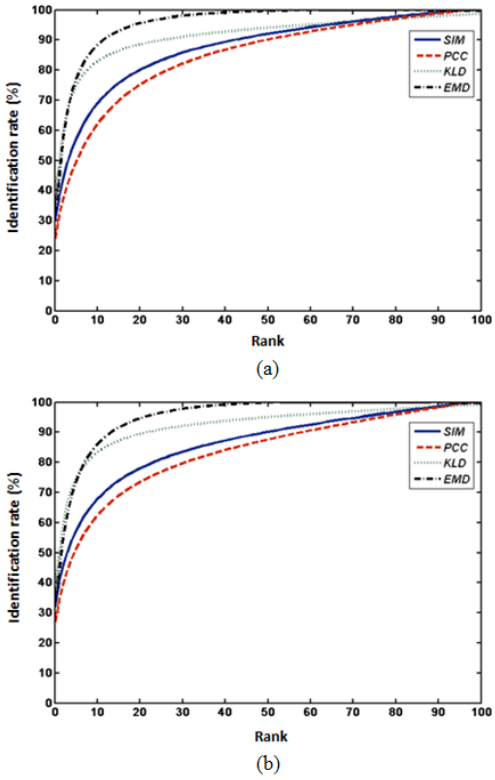


Fig. 7. Cumulative Match Characteristic (CMC) curves for datasets (a) VD1 and (b) VD2 (using the best performing fusion scheme for every case).

### C. *Information Fusion from Different Datasets*

During our research we decided to test the behavior of the suggested scheme during the combination of information coming from enrollments that correspond to different visual content. Since the constructed datasets VD1, VD2 correspond to different spatio-temporal layouts, their samples are combined at the match score level. For implementing this particular scenario we feed the fusion module with the pairwise match scores calculated for the respective time interval FDMs coming from both datasets. During our experiments we employed the same fusion schemes that were utilized in the previous cases (*SM*, *WM*, *LR*).

In Table III we can observe the resulting EERs after information fusion from datasets VD1, VD2 and Table IV presents the corresponding values for the calculated Rank-1 IRs. Similarly, in Fig. 8 we present a general overview of performance during match score fusion from the two datasets, both for the case of a verification (ROC curves) and an identification (CMC curves) scenario.

TABLE III

EQUAL ERROR RATES

| Fusion of information from VD1 and VD2 | | | | |
|---|---|---|---|---|
| Fusion | Comparison Measure | | | |
| | *SIM* | *PCC* | *KLD* | *EMD* |
| *SM* | 26.2% | 27.5% | 20.1% | 15.3% |
| *WM* | 26.7% | 28.6% | 23.0% | 21.1% |
| *LR* | **25.8%** | **26.7%** | **19.3%** | **10.8%** |

TABLE IV

RANK-1 IDENTIFICATION RATES

| Fusion of information from VD1 and VD2 | | | | |
|---|---|---|---|---|
| Fusion | Comparison Measure | | | |
| | *SIM* | *PCC* | *KLD* | *EMD* |
| *SM* | 38.7% | 32.7% | **51.0%** | 38.0% |
| *WM* | 23.2% | 16.7% | 31.5% | 21.5% |
| *LR* | **41.6%** | **33.1%** | 44.7% | **43.6%** |

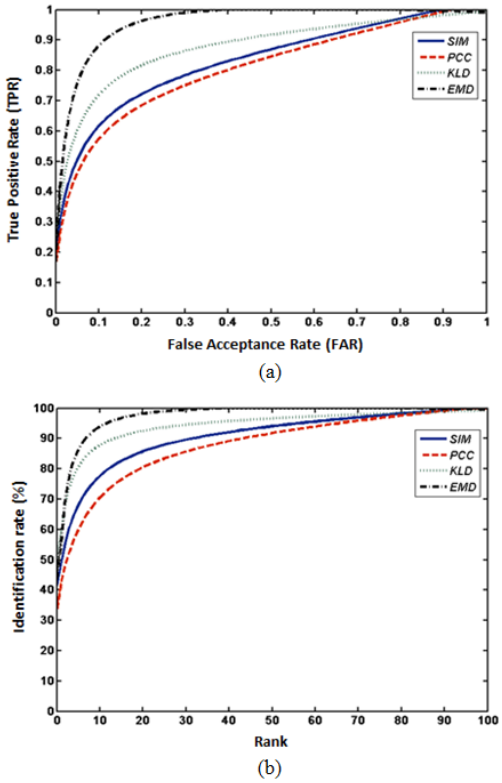


Fig. 8. (a) Receiver Operating Characteristic (ROC) and (b) Cumulative Match Characteristic (CMC) curves for match score fusion from datasets VD1 and VD2 (using the best performing fusion scheme for every case).

## D. Database Scaling Performance

In order to examine the impact of database scaling, i.e. performance behavior by increasing the number of subjects, we generated random subsets from the complete database of 200 subjects, and calculated biometric performance for sets VD1, VD2, and their fusion. Fig. 9 depicts the obtained results. The variation in EER is relatively minor, since relative difference for the extreme values (50 and 200 subjects) is less than 15% on average. The corresponding Rank-1 IR degrades substantially when increasing the number of subjects. For the relative small group of 50 subjects, the Rank-1 IR is 52.9% for VD1, 53.7% for VD2 and 61.2% for the fusion case. For the complete database of 200 subjects, corresponding rates are 32.5%, 32.8%, and 43.6%. Therefore, this is a relative degradation in performance of 38.5% for VD1, 38.9% for VD2, and 28.7% for the combination of the two datasets.

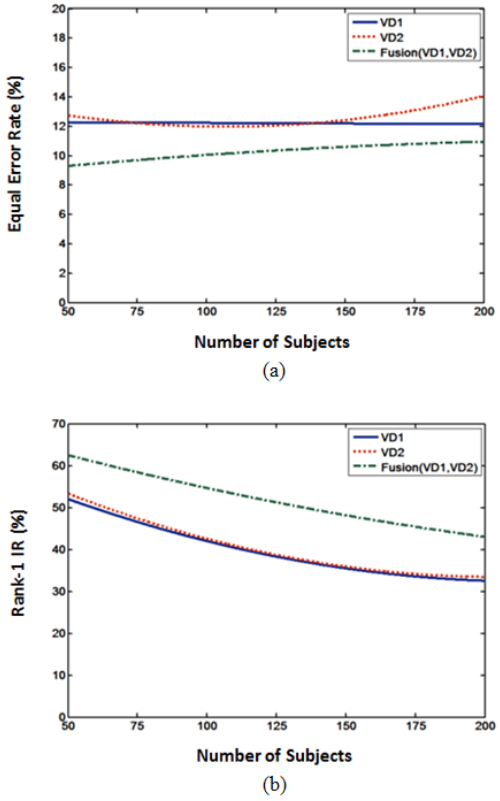


Fig. 9. (a) EER and (b) Rank-1 IR performances while increasing the number of subjects in database.

## E. Behavior under Temporal Resolution Degradation

During our experiments, we decided to explore the tolerance of the proposed methods to setups that have limited sampling rate by artificially changing the temporal resolution of the captured eye movement signal. This investigation is very important for the future development of eye movement-driven biometric methods that would run in tandem with iris recognition techniques on the existing iris recognition hardware. The eye image sampling frequency of the iris recognition devices frequently has an upper boundary of 30Hz, which is much lower than the commercial high-grade eye tracking equipment that is able to capture eye images at rates up to 2000Hz [46].

In order to perform a comparative evaluation with existing eye movement-driven biometric techniques we utilized two approaches, (CEM-P) [34] and (CEM-B) [36], that have been previously evaluated in scenarios of reduced sampling frequency. We used the same sampling frequency tiers that were employed in the papers describing CEM-P and CEM-B ([34], [36]), and specifically: 1000 Hz (the original sampling frequency), 500 Hz, 250 Hz, 120 Hz, 75 Hz and 30 Hz. In the case of the current approach (denoted *FDM-EMD*), we used the best performing comparison measure (*EMD*) and the best fusion strategy (*LR*).

Fig. 10 illustrates the behavior of the inspected methods by successively degrading the frequency resolution both for a verification (EER) and an identification (Rank-1 IR) scenario. In the most extreme case of frequency resolution degradation (30 Hz) the EER for the presented method increases from

12.1% to 14.6% (a relative increment of 20.6%), whereas for CEM-P it rises from 31.4% to 40.7% (a relative increment of 29.6%) and for CEM-B from 21.9% to 30% (relative increment of 37%). In the case of the identification scenario, the superiority of the proposed approach is again prominent. For the suggested scheme, Rank-1 IR decreases from 32.5% to 26.7% (a relative loss of 17.8%), whereas for the case of CEM-P falls from 10.4% to 2.5% (a relative loss of 76.0%), and for CEM-B from 27.4% to 8.7% (a relative loss of 68.2%).

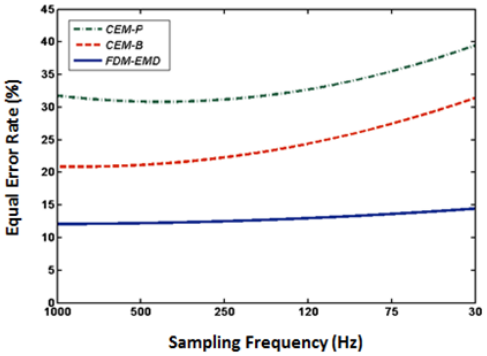


(a)

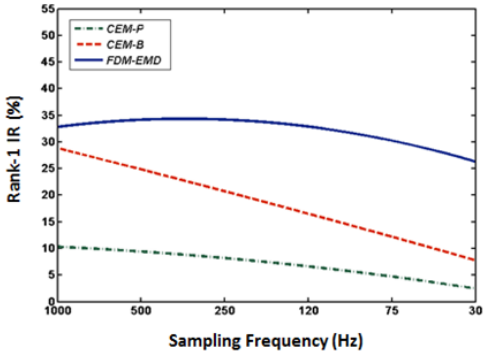


(b)

Fig. 10. (a) EER and (b) Rank-1 IR performances in case of temporal resolution degradation.

## VI. Discussion

### A. Performance Characteristics

The main target of the conducted study was to develop and evaluate a generalized framework for the representation and comparison of spatial distributions formed by eye movements in a time-changing visual environment. We assessed the performance of FDM-based biometric templates using four different comparison schemes and three fusion approaches. The evaluation results reveal that under a verification scenario the EER tops on a value of 12.1%, whereas in case of an identification scenario the highest achieved Rank-1 IR is 39.4%. Our experiments showed that the identification performance can be further improved by combining the information coming from recordings of the same person. In such cases, the EER improved to 10.8% and Rank-1 IR to 51.0%. These performances constitute a substantial progress in the field of eye movement biometrics, since the achieved EERs outperform all the previous reported values for the method described in papers [30], [32], [33], [34], [35], [36]. The importance of the results may be emphasized by the fact that the method was evaluated on a large data pool formed from 200 subjects. It should be noted, though, that the reported performances are still inferior to those achieved by well-established biometric methods (e.g. fingerprints and iris) capable to deliver EER < 2%. In addition, the overlap in distributions of *genuine* and *impostor* match scores, depicted in Fig. 5, implies a sensitivity that would probably obscure a straightforward utilization of the specific feature as a standalone trait in a high precision biometric system.

During our analysis we investigated four computational schemes that can be used for the comparison of FDMs. A close inspection of Tables I, II, III, and IV reveals that the utilized dissimilarity measures (Kullback-Leibler Divergence and Earth Mover's Distance) outperform the similarity measures (Similarity metric and Pearson's Correlation Coefficient) in every case. These differences in performance are additionally confirmed by the results of the one-way ANOVA across the comparison schemes. Earth Mover's Distance achieved better rates in the majority of the considered scenarios and appears as the preferable choice in terms of recognition accuracy. Nevertheless, a time consumption analysis implemented for the evaluated measures and presented in Fig. 11, reveals that Earth Mover's Distance requires substantially more computational time than the other measures for a pairwise comparison of two FDMs. As a result, Kullback-Leibler Divergence may appear as a more feasible solution in the eye movement-driven biometric systems where a good trade-off between computational load and performance is of major concern.

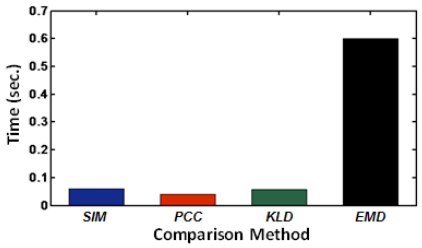


Fig. 11. Comparison of computational delays for the employed schemes (simulations implemented in an Intel Core2 Quad Q9400, 2.66GHz, 8GB RAM. Time averaged over 100 iterations).

Combination of the individual time interval FDMs was accomplished by conducting fusion in the match score level using three different schemes: Simple Mean (*SM*), Weighted Mean (*WM*), and Likelihood Ratio (*LR*). The exact same schemes were also used for the combination of information coming from both datasets. Likelihood Ratio (*LR*) demonstrated superior performance in all cases for the measure of EER. For the case of Rank-1 IR, *LR* scheme was outperformed only once, in the case of *KLD* measure where the Simple Mean (*SM*) scheme achieved better rates. It is worth commenting that the Weighted Mean (*WM*) scheme failed to generate competitive results. This may lead to the conclusion that, in general, there is no preferred feature map for a specific time interval that should be accounted at the expense of the others, something that is also supported by the results of the one-way ANOVA across different time interval maps.

### B. Dynamic Update of Biometrical Templates

The conducted experiments revealed the capability to boost the identification rates with the combination of enrollments corresponding to different visual content. Apart from the desirable performance gain, this characteristic has another significant effect since it may be exploited in order to provide anti-spoofing robustness to a biometric system. In some established methods (e.g. fingerprints, iris) once an exact replica of the biometric feature is acquired it can then be routinely used to perform multiple spoof attacks. In the case of FDMs, however, this 'once fooled always fooled' state might be negated. Even if someone is able to replicate the fixation distributions formed for a certain visual stimulus, the template can be periodically enhanced or even totally updated with the use of a new enrollment corresponding to different visual content.

### C. Robustness to Temporal Signal Distortions

During our research we evaluated the tolerance of the proposed scheme in case of temporal resolution degradation. The results presented in Fig. 10 demonstrate the robustness of the proposed scheme to such effects. In comparison to the other methods that also rely on eye movements ([34], [36]), the relative loss in performance is lower both for the case of EER and for Rank-1 IR. This optimum behavior can be attributed mainly to two reasons: first, FDMs mostly represent spatial characteristics and thus the effects of temporal degradation affect the constructed templates at a lower degree, second, any minor misalignments in the exact locations of fixation points can be effectively blended in the probabilistic representation of a FDM.

Fig. 12 portrays the effect of decreasing the sampling frequency on FDMs representation. Despite observed influence from the reduction in temporal resolution, the main characteristics of fixation distributions are still preserved in the biometric template.

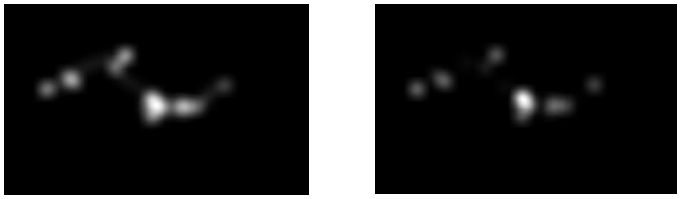

(a) (b)

Fig. 12. Influence of temporal resolution degradation to FDM representation. The presented FDMs correspond to the same recording, sampled with frequencies: (a) 1000 Hz and (b) 30 Hz.

### D. Limitations

The presented results should be evaluated under the scope of certain limitations. First, recordings for every subject were implemented during the same day and consequently template aging is a phenomenon that might possibly affect FDM features for samples recorded at much greater time intervals. Furthermore, the databases were constructed using two samples per subject. The performance (either better or worse) in case of more viewings of the same content is still an unexplored field. Second, the experiments were conducted in a lab-controlled environment using a chin-rest with head bar to ensure the highest possible quality for the recordings. In a real-world system though, utilization of a chin-rest might be an infeasible option. However, this limitation could be surpassed with the utilization of a system configuration that consists of two (or more) light sources and/or cameras, allowing thus for a larger degree of freedom for head movements [47]. Finally, it should be mentioned that several behavior changing conditions, e.g., stress, alcohol etc., could potentially influence the formation of fixation patterns and as a result the corresponding biometric templates.

## VII. Conclusion

In this paper we presented a general framework based on Fixation Density Maps (FDMs) for the representation of eye movements recorded under the influence of dynamic visual stimulus. Our research included a thorough investigation of different comparison schemes that can be employed for assessing the similarity of the constructed multi-map biometric templates. In addition, various fusion schemes were explored for the task of effectively combining the similarity information coming from different FDMs in the match score level. To this point, the achieved identification rates suggest a possible employment of the proposed scheme as an assistive biometrical trait in security systems by exploiting in parallel its advantageous properties such as the capability of dynamically enhancing biometric templates.

In our future work, we intend to explore the possibility of combining the proposed scheme with techniques that represent primarily temporal characteristics in order to investigate its benefits in terms of performance and stability in a biometric system that depends solely on eye movement traits.

## References


[1] D. Maio, D. Maltoni, R. Cappelli, J. L. Wayman, and A. K. Jain, "FVC2004: Third Fingerprint Verification Competition," in *Biometric Authentication*. vol. 3072, D. Zhang and A. K. Jain, Eds., ed: Springer Berlin Heidelberg, 2004, pp. 1-7.

[2] M. J. Burge and K. W. Bowyer, *Handbook of Iris Recognition*: Springer Publishing Company, Incorporated, 2013.

[3] S. Z. Li and A. K. Jain, *Handbook of Face Recognition*: Springer Publishing Company, Incorporated, 2011.

[4] S. Venugopalan and M. Savvides, "How to Generate Spoofed Irises From an Iris Code Template," *Information Forensics and Security, IEEE Transactions on,* vol. 6, pp. 385-395, 2011.

[5] R. N. Rodrigues, N. Kamat, and V. Govindaraju, "Evaluation of biometric spoofing in a multimodal system," in *Biometrics: Theory Applications and Systems (BTAS), 2010 Fourth IEEE International Conference on*, 2010, pp. 1-5.

[6] A. Kumar and D. Zhang, "Personal recognition using hand shape and texture," *Image Processing, IEEE Transactions on,* vol. 15, pp. 2454-2461, 2006.

[7] D. Zhang, W. Zuo, and F. Yue, "A Comparative Study of Palmprint Recognition Algorithms," *ACM Comput. Surv.,* vol. 44, pp. 1-37, 2012.

[8] L. Chih-Lung and F. Kuo-Chin, "Biometric verification using thermal images of palm-dorsa vein patterns," *Circuits and Systems for Video Technology, IEEE Transactions on,* vol. 14, pp. 199-213, 2004.

[9] N. Houmani, A. Mayoue, S. Garcia-Salicetti, B. Dorizzi, M. I. Khalil, M. N. Moustafa*, et al.*, "BioSecure signature evaluation campaign (BSEC'2009): Evaluating online signature algorithms depending on the quality of signatures," *Pattern Recognition,* vol. 45, pp. 993-1003, 2012.

[10] T. Kinnunen and H. Li, "An overview of text-independent speaker recognition: From features to supervectors," *Speech Commun.,* vol. 52, pp. 12-40, 2010.

[11] M. Karnan, M. Akila, and N. Krishnaraj, "Biometric personal authentication using keystroke dynamics: A review," *Applied Soft Computing,* vol. 11, pp. 1565-1573, 2011.

[12] S. Sarkar, P. J. Phillips, Z. Liu, I. R. Vega, P. Grother, and K. W. Bowyer, "The humanID gait challenge problem: data sets, performance, and analysis," *Pattern Analysis and Machine Intelligence, IEEE Transactions on,* vol. 27, pp. 162-177, 2005.

[13] *Google Glass*. Available: http://www.google.com/glass/start/

[14] O. V. Komogortsev and A. Karpov, "Liveness detection via oculomotor plant characteristics: Attack of mechanical replicas," in *Biometrics (ICB), 2013 International Conference on*, 2013, pp. 1-8.

[15] O. V. Komogortsev, A. Karpov, C. D. Holland, and H. P. Proenca, "Multimodal ocular biometrics approach: A feasibility study," in *Biometrics: Theory, Applications and Systems (BTAS), 2012 IEEE Fifth International Conference on*, 2012, pp. 209-216.

[16] K. Hollingsworth, K. W. Bowyer, and P. J. Flynn, "Identifying useful features for recognition in near-infrared periocular images," in *Biometrics: Theory Applications and Systems (BTAS), 2010 Fourth IEEE International Conference on*, 2010, pp. 1-8.

[17] H. Drira, B. Ben Amor, A. Srivastava, and M. Daoudi, "A Riemannian analysis of 3D nose shapes for partial human biometrics," in *Computer Vision, 2009 IEEE 12th International Conference on*, 2009, pp. 2050-2057.

[18] Y. F. Liu, L. Chao-Yu, and J. M. Guo, "Impact of the Lips for Biometrics," *Image Processing, IEEE Transactions on,* vol. 21, pp. 3092-3101, 2012.

[19] R. J. Leigh and D. S. Zee, *The Neurology of Eye Movements, 4th ed.*: London, U.K, Oxford Univ. Press, 2006.

[20] M. Carrasco, "Visual attention: The past 25 years," *Vision Research,* vol. 51, pp. 1484-1525, 2011.

[21] A. T. Bahill, "Development, validation, and sensitivity analyses of human eye movement models," *Crit Rev Bioeng,* vol. 4, pp. 311-55, 1980.

[22] D. Noton and L. Stark, "Scanpaths in eye movements during pattern perception," *Science (New York, N.Y.),* vol. 171, pp. 308-311, 1971.

[23] D. Noton and L. Stark, "Scanpaths in saccadic eye movements while viewing and recognizing patterns," *Vision Research,* vol. 11, pp. 929-932, 1971.

[24] G. J. Walker-Smith, A. G. Gale, and J. M. Findlay, "Eye movement strategies involved in face perception," *Perception,* vol. 6, pp. 313-326, 1977.

[25] L. W. Stark and S. R. Ellis, "Scanpaths revisited: cognitive models direct active looking," in *Eye movements: cognition and visual perception*, D. F. Fisher, Ed., ed: Lawrence Erlbaum Associates, 1981, pp. 193-226.

[26] T. Foulsham and G. Underwood, "What can saliency models predict about eye movements? Spatial and sequential aspects of fixations during encoding and recognition," *Journal of Vision,* 2008.

[27] S. K. Mannan, K. H. Ruddock, and D. S. Wooding, "Fixation sequences made during visual examination of briefly presented 2D images," *Spatial Vision,* vol. 11, pp. 157-178, 1997.

[28] S. Josephson and M. E. Holmes, "Visual attention to repeated internet images: testing the scanpath theory on the world wide web," in *2002 Symposium on Eye Tracking Research & Applications (ETRA 2002)*, New Orleans, Louisiana, 2002, pp. 43-49.

[29] P. Kasprowski and J. Ober, "Eye Movements in Biometrics," in *Biometric Authentication*. vol. 3087, D. Maltoni and A. K. Jain, Eds., ed: Springer Berlin Heidelberg, 2004, pp. 248-258.

[30] T. Kinnunen, F. Sedlak, and R. Bednarik, "Towards task-independent person authentication using eye movement signals," in *2010 Symposium on Eye Tracking Research & Applications (ETRA 2010)*, Austin, Texas, 2010, pp. 187-190.

[31] O. V. Komogortsev, A. Karpov, L. R. Price, and C. Aragon, "Biometric authentication via oculomotor plant characteristics," in *Biometrics (ICB), 2012 5th IAPR International Conference on*, 2012, pp. 413-420.

[32] I. Rigas, G. Economou, and S. Fotopoulos, "Biometric identification based on the eye movements and graph matching techniques," *Pattern Recognition Letters,* vol. 33, pp. 786-792, 2012.

[33] O. V. Komogortsev and C. D. Holland, "Biometric Authentication via Complex Oculomotor Behavior," in *Biometrics: Theory, Applications and Systems (BTAS), 2013 IEEE Sixth International Conference on*, 2013, pp. 1-8.

[34] C. D. Holland and O. V. Komogortsev, "Complex Eye Movement Pattern Biometrics: The Effects of Environment and Stimulus," *Information Forensics and Security, IEEE Transactions on,* vol. 8, pp. 2115-2126, 2013.

[35] C. D. Holland and O. V. Komogortsev, "Biometric identification via eye movement scanpaths in reading," in *2011 International Joint Conference on Biometrics*, 2011, pp. 1-8.

[36] C. D. Holland and O. V. Komogortsev, "Complex eye movement pattern biometrics: Analyzing fixations and saccades," in *Biometrics (ICB), 2013 International Conference on*, 2013, pp. 1-8.

[37] I. Rigas and O. V. Komogortsev, "Biometric Recognition via fixation density maps," in *SPIE 9075, Biometric and Surveillance Technology for Human and Activity Identification XI, 90750M*, 2014.

[38] O. Le Meur and T. Baccino, "Methods for comparing scanpaths and saliency maps: strengths and weaknesses," *Behavior Research Methods,* vol. 45, pp. 251-266, 2013.

[39] N. Riche, M. Duvinage, M. Mancas, B. Gosselin, and T. Dutoit, "Saliency and Human Fixations: State-of-the-art and Study of Comparison Metrics," in *IEEE 13th International Conference on Computer Vision* 2013.

[40] T. Judd, F. Durand, and A. Torralba, "A benchmark of computational models of saliency to predict human fixations," MIT, Technical Report MIT-CSAIL-TR-2012-001, 2012.

[41] S. Kullback and R. A. Leibler, "On Information and Sufficiency," *The Annals of Mathematical Statistics,* vol. 22, pp. 79-86, 1951.

[42] F. L. Hitchcock, "The distribution of a product from several sources to numerous localities," *Journal of Math. Phys.,* vol. 20, pp. 224-230, 1941.

[43] E. Pekalska, P. Paclik, and R. P. W. Duin, "A generalized kernel approach to dissimilarity-based classification," *J. Mach. Learn. Res.,* vol. 2, pp. 175-211, 2002.

[44] Y. Chen, E. K. Garcia, M. R. Gupta, A. Rahimi, and L. Cazzanti, "Similarity-based Classification: Concepts and Algorithms," *J. Mach. Learn. Res.,* vol. 10, pp. 747-776, 2009.

[45] K. Nandakumar, C. Yi, S. C. Dass, and A. K. Jain, "Likelihood Ratio-Based Biometric Score Fusion," *Pattern Analysis and Machine Intelligence, IEEE Transactions on,* vol. 30, pp. 342-347, 2008.

[46] *EyeLink. EyeLink 1000 Eye Tracker*. Available: http://www.sr-research.com/

[47] E. D. Guestrin and E. Eizenman, "General theory of remote gaze estimation using the pupil center and corneal reflections," *Biomedical Engineering, IEEE Transactions on,* vol. 53, pp. 1124-1133, 2006.

Ioannis Rigas received his Ph.D. degree from the Department of Physics, University of Patras, Greece, in 2013. Currently, he is a Postdoctoral Research Associate at Department of Computer Science, Texas State University, San Marcos, Texas, USA. His current research interests involve eye movement modeling and simulation with application on the field of biometric recognition and anti-spoof protection.

Oleg Komogortsev received his Ph.D. degree from the Department of Computer Science at Kent State University in 2007. Currently, he is an Associate Professor at Department of Computer Science, Texas State University, San Marcos, Texas, USA. His research interests are eye tracking, biometrics, human computer interaction, and bioengineering. He is a recipient of an NSF CAREER award.